Analysis of Secondary Structure Effects on the IR and Raman Spectra of Polypeptides in Terms of Localized Vibrations

Christoph R. Jacob,* Sandra Luber, and Markus Reiher*

ETH Zurich, Laboratorium für Physikalische Chemie, Wolfgang-Pauli-Strasse 10, 8093 Zurich, Switzerland

Received: January 13, 2009; Revised Manuscript Received: March 3, 2009

We demonstrate how the recently developed methodology for the analysis of calculated vibrational spectra in terms of localized modes [*J. Chem. Phys.* **2009**, *130*, 084106] can be applied to investigate the influence of the secondary structure on infrared and Raman spectra of polypeptides. As a model system, a polypeptide consisting of 20 (S)-alanine residues in the conformation of an α-helix and of a 3_{10}-helix is considered. Several features of the calculated spectra are analyzed in detail. First, we show for the amide II band how localized modes facilitate the decomposition of the total Raman intensities into contributions of certain groups of atoms, and how such an analysis can be used to identify the origin of differences in Raman intensity of the two helices. Second, we demonstrate how the shift of the position of the amide I band between the two considered structures can be rationalized and how the observed intensity distribution within the amide I band can be explained by considering the coupling constants between the localized modes. Third, we show how localized modes can be employed to analyze the positions of the bands found in the extended amide III region and how such an analysis makes it possible to gain a better understanding of how structural changes influence the coupling between the amide III and the $C^{\alpha}-H$ bending modes in this region.

1. Introduction

The determination of the structure of proteins and other biomolecules is a prerequisite for the understanding of most biochemical processes. While X-ray crystallography and NMR spectroscopy often provide detailed structural information, there are several cases where these techniques cannot be employed. Therefore, other complementary spectroscopic methods are needed. Vibrational spectroscopy provides such a method that allows one to study the structure of proteins in their natural environment (i.e., in aqueous solution). In particular, infrared (IR) and Raman spectroscopy (for reviews, see, e.g., refs 1–4) as well as their chiral variants vibrational circular dichroism (VCD) and Raman optical activity (ROA) spectroscopy (for reviews, see, e.g., refs 5 and 6) have been used extensively to investigate the structure of proteins.

However, while X-ray crystallography and NMR spectroscopy provide structural information rather directly, in vibrational spectroscopy this information has to be extracted from the measured vibrational frequencies and intensities. Therefore, it is crucial to understand how the measured vibrational spectra are determined by the structure of the investigated protein, and how changes in the secondary structure influence the positions and intensities of the bands in the vibrational spectra. To relate protein structure and vibrational spectra, dedicated experimental studies on model peptides as well as detailed theoretical investigations are necessary.[7] One particular example where such a link could be established is the discrimination of α-helix and 3_{10}-helix by means of IR and VCD spectroscopy. Using a combination of experiment and theory, Keiderling and coworkers showed that the two conformations can be clearly distinguished by a specific VCD pattern in the amide I and amide II regions.[8] Another example is the absolute conformation of tryptophan side chains, which can be determined from the sign of a particular band in the ROA spectrum, as was recently shown both experimentally and theoretically.[9,10]

For a detailed understanding of the relation between secondary structure and vibrational spectra, ab initio calculations are extremely useful.[7] They allow it to study well-defined structural models that can be varied in a controlled way. This makes it possible to isolate the secondary structure changes from other effects, thus providing insight that is not available from experimental studies, where changes in secondary structure always go along with other changes, such as, for example, changes of the primary structure or of the solvent.

However, while accurate calculations of vibrational spectra of molecules containing hundreds of atoms are nowadays possible with efficient quantum-chemical methodology (for examples, see, refs 11–13) (if necessary in combination with a selective calculation of specific normal modes[14,15] or of normal modes with a high intensity),[16,17] the interpretation of the results of such large calculations remains difficult. For polypeptides and proteins, the calculated spectra usually comprise a large number of close lying normal modes that are delocalized combinations of vibrations on different amino acid residues. However, since these individual normal modes are usually not resolved in experiment, many of them contribute to one band in the observed vibrational spectrum. This makes it difficult to analyze how structural changes influence the positions and intensities of the observed bands and to extract general rules relating secondary structure and vibrational spectra.

To overcome this problem, we recently developed a methodology for the analysis of calculated vibrational spectra in terms of localized modes.[18] For a given set of normal modes, usually those modes that contribute to a certain band in the vibrational spectrum, the localized modes are obtained by determining a unitary transformation that leads to the modes that maximize a suitably defined localization criterion. In contrast to the delocalized normal modes, these localized modes will in general

* To whom correspondence should be addressed. E-mail: (C.R.J.) christoph.jacob@phys.chem.ethz.ch; (M.R.) markus.reiher@phys.chem.ethz.ch.

10.1021/jp900354g CCC: $40.75
Published on Web 04/10/2009

be dominated by a vibration on one single residue, and localized modes on different but homologous residues will be very similar. Therefore, the localized modes simplify the interpretation of calculated vibrational spectra of polypeptides and proteins and make it possible to rationalize the effects of structural changes by considering the changes of the vibrational frequencies and intensities of the localized modes as well as the changes of the couplings between them. Note that with our methodology it is possible to extract localized modes and coupling constants from accurate calculations on full polypeptides or proteins, thus avoiding the crude approximations that are made if local modes and coupling constants obtained from calculations on small model systems or from empirical models are employed.

Here, we apply our newly developed methodology for the analysis of vibrational spectra in terms of localized modes to study the IR and Raman spectra of a helical polypeptide consisting of 20 (S)-alanine residues for which an α-helical and a 3_{10}-helical conformation will be compared. These examples have been chosen since they can serve as a model for more complicated proteins, and because they allow us to demonstrate how localized modes can be employed for analyzing the effects of secondary-structure changes on the vibrational spectra of polypeptides and proteins.

This work is organized as follows. In Section 2.1, the theoretical background is briefly reviewed. This is followed by a discussion of the analysis of vibrational intensities and band shapes in terms of localized modes in Section 2.2. The computational details are given in Section 3, and the results obtained for α-helical and 3_{10}-helical alanine polypeptides are presented in Section 4. In particular, in Section 4.3 the change of the Raman intensity of the amide II band is investigated, in Section 4.4 the shift of the position of the amide I band is analyzed, and in Section 4.5 the coupling between N−H bending and C^{α}−H bending vibrations in the extended amide III region is studied. Finally, a summary and concluding remarks are given in Section 5.

2. Theory

2.1. Localization of Normal Modes. Within the harmonic approximation, the normal modes and vibrational frequencies can be obtained by diagonalizing the mass-weighted molecular Hessian matrix $\mathbf{H}^{(m)}$, which contains the second derivatives of the total electronic energy E (including the nuclear repulsion energy) with respect to Cartesian nuclear coordinates,[7] that is

$$\mathbf{H}^{(m)}_{i\alpha,j\beta} = \frac{1}{\sqrt{m_i m_j}}\left(\frac{\partial^2 E}{\partial R_{i\alpha}\partial R_{j\beta}}\right)_0 \tag{1}$$

where the subscript "0" denotes that the derivative is evaluated at the equilibrium structure $\boldsymbol{R_0}$. In the above expression, m_i is the atomic mass of nucleus i, and $R_{i\alpha}$ is the $\alpha = x,y,z$ Cartesian component of the position of nucleus i. The matrix $\mathbf{Q}$ containing the eigenvectors of $\mathbf{H}^{(m)}$ can be employed to transform the Hessian matrix to diagonal form,

$$\mathbf{H}^{(q)} = \mathbf{Q}^T\mathbf{H}^{(m)}\mathbf{Q} \tag{2}$$

where $\mathbf{H}^{(q)}$ is a diagonal matrix with the diagonal elements (i.e., the eigenvalues of $\mathbf{H}^{(m)}$) equal to the squares of the angular frequencies, $H^{(q)}_{pp} = \omega_p^2 = 4\pi^2\nu_p^2$, with vibrational frequencies ν_p. The columns of the matrix $\mathbf{Q}$ are the normal modes in terms of mass-weighted Cartesian displacements. These normal modes will be referred to as $\mathbf{Q}_p$, and its components as $Q_{i\alpha,p}$. The $\mathbf{Q}_p$ are chosen to be normalized, that is, $|\boldsymbol{Q}_p|^2 = \Sigma_{i\alpha}Q^2_{i\alpha,p} = 1$, so that the matrix $\mathbf{Q}$ is unitary. The normal modes in terms of not mass-weighted Cartesian displacements $\mathbf{Q}^{(c)}_p$, can be obtained as $Q^{(c)}_{i\alpha,p} = (1/m_i^{1/2})Q_{i\alpha,p}$.

In order to analyze the vibrational spectra of polypeptides and proteins in terms of localized modes,[18] one considers a subset of k normal modes, which are usually those modes that contribute to one band in the vibrational spectrum. These normal modes are collected in the matrix $\mathbf{Q}^{\mathrm{sub}}$. By means of a unitary transformation U, these can be transformed to a set of localized modes

$$\tilde{\mathbf{Q}}^{\mathrm{sub}} = \mathbf{Q}^{\mathrm{sub}}U \tag{3}$$

where the unitary transformation is chosen such that it yields the "most localized" transformed modes. This is achieved by maximizing $\xi(\tilde{\mathbf{Q}}^{\mathrm{sub}}) = \xi(\mathbf{Q}^{\mathrm{sub}}U)$, where $\xi(\tilde{\mathbf{Q}}^{\mathrm{sub}})$ is a suitably defined criterion that measures how localized a set of transformed modes $\tilde{\mathbf{Q}}^{\mathrm{sub}}$ is.[18] Here and in the following, the tilde is used to denote the localized modes, or other quantities that are defined with respect to these localized modes. The localizing unitary transformation U can then be determined using the Jacobi-sweep method as discussed in ref 18.

For the localization criterion $\xi(\tilde{\mathbf{Q}}^{\mathrm{sub}})$, different definitions can be employed. Here, we will use the atomic-contribution criterion[18]

$$\xi_{\mathrm{at}}(\tilde{\mathbf{Q}}^{\mathrm{sub}}) = \sum_{p=1}^{k}\sum_{i=1}^{n}(\tilde{C}^{\mathrm{sub}}_{ip})^2 \tag{4}$$

where $\tilde{C}^{\mathrm{sub}}_{ip}$ is the contribution of nucleus i to the mode $\tilde{\mathbf{Q}}^{\mathrm{sub}}_p$, which can be measured by the fraction of the kinetic energy of this atom in the normal mode as [19–21]

$$\tilde{C}^{\mathrm{sub}}_{ip} = \sum_{\alpha=x,y,z}(\tilde{Q}^{\mathrm{sub}}_{i\alpha,p})^2 \tag{5}$$

This criterion measures the number of atomic centers that contribute to each of the modes. It leads to localized modes to which as few atomic centers as possible contribute.

Note that the localized modes are not eigenvectors of the mass-weighted Hessian $\mathbf{H}^{(m)}$, and therefore have no direct physical significance. Nevertheless, they can be useful for the interpretation of calculated vibrational spectra. For polypeptides and proteins, where the normal modes are in general delocalized combinations of vibrations on different amino acid residues, the localized modes will each be dominated by a vibration of one single residue. Furthermore, the localized modes on different residues will involve similar atomic displacements, that is, the set of localized modes obtained for one vibrational band will consist of modes that are very similar but are located on different residue. This very simple structure of the localized modes makes them well suited for the analysis of vibrational spectra and, as will be discussed in the following, makes it possible to analyze the positions and intensities as well as shapes of the bands in the vibrational spectra.

In order to analyze the positions and shapes of the bands in the vibrational spectra, it is useful to define the (vibrational) coupling matrix $\tilde{\mathbf{\Omega}}$ as[18]

$$\tilde{\mathbf{\Omega}} = \mathbf{U}^T\mathbf{\Omega}\mathbf{U} \tag{6}$$

where $\mathbf{\Omega}$ is a diagonal matrix with the vibrational frequencies $\nu_p = \omega_p/2\pi$ of the considered normal modes on the diagonal. From this coupling matrix $\tilde{\mathbf{\Omega}}$, the vibrational frequencies of the normal modes and the transformation matrix $\mathbf{U}$ can be obtained by diagonalization. The eigenvectors of $\tilde{\mathbf{\Omega}}$ are the rows of the transformation matrix $\mathbf{U}$ (columns of the inverse transformation $\mathbf{U}^T$) and give the composition of the normal modes in the basis of localized modes.

As is discussed in ref 18, the diagonal elements $\tilde{\Omega}_{pp}$ of this coupling matrix can be interpreted as vibrational frequencies of the localized modes. For a set of localized modes that are similar but located on different residues, these frequencies of the localized modes will be very similar, that is, the localized modes are energetically (almost) degenerate. As will be shown, a shift in the position of a band in the vibrational spectrum can then be understood in terms of a shift of the frequencies of the localized modes. Since these localized modes are very similar, it will be sufficient to consider only one representative localized mode for analyzing this shift.

The off-diagonal elements $\tilde{\Omega}_{pq}$ can be understood as coupling constants. In the case of two degenerate localized modes, the magnitude of the corresponding coupling constant corresponds to half the frequency splitting between two normal modes that arise as combination of these localized modes. For nondegenerate localized modes and for a larger number of localized modes, more complicated coupling patterns arise. However, the resulting vibrational frequencies of the normal modes can still be understood in terms of the frequencies of the localized modes $\tilde{\Omega}_{pp}$ and the coupling constants $\tilde{\Omega}_{pq}$ between them. Note that the coupling constants $\tilde{\Omega}_{pq}$ will in general be small for localized modes that are centered on groups which are not spatially close. Consequently, for each localized mode only couplings with a small number of other modes will be significant. Furthermore, in the case of polypeptides and proteins, the coupling constants between localized modes on neighboring residues in similar secondary structure elements will be very similar. Therefore, the coupling matrix $\tilde{\mathbf{\Omega}}$ in general has a rather simple structure, which allows us to understand how the more complicated delocalized normal modes arise.

2.2. Analysis of Vibrational Intensities in Terms of Localized Modes. The vibrational frequencies of the localized modes and the coupling constants between the localized modes can be used to analyze the positions of the bands in the vibrational spectrum. In addition, the localized modes can also be employed for analyzing both the total intensities of these bands as well as their band shapes. This will be investigated now for the total band intensities and in the following section for the band shapes.

In IR spectroscopy, the absorption of the p-th vibrational mode is proportional to the square of the derivative of the dipole moment with respect to the corresponding normal mode[11]

$$\mathcal{A}_p^{\mathrm{IR}} \propto \left(\frac{\partial \boldsymbol{\mu}}{\partial \mathbf{Q}_p}\right)_0^2 = \sum_{\alpha} \left(\frac{\partial \mu_\alpha}{\partial \mathbf{Q}_p}\right)_0^2 \tag{7}$$

and the scattering intensity measured in Raman spectroscopy is proportional to a linear combination of the Raman invariants[22,11]

$$I_p^{\mathrm{Raman}} \propto [c_1 a_p^2 + c_2 {\gamma_p}^2] \tag{8}$$

where the coefficients c_1 and c_2 depend on the geometry of the scattering experiment. For the most common case in which the incident light is linearly polarized and the scattered light is detected at an angle of 90°, one has $c_1 = 45$ and $c_2 = 7$.[22] The term on the right-hand side is the so-called scattering factor S. Since the proportionality constant in the above expression depends on the precise experimental conditions (for details, see refs 11 and 23) it is common, in particular in theoretical studies, to ignore this proportionality constant and to consider only the Raman scattering factor S. The isotropic and anisotropic Raman invariants are given by[22]

$$a_p^2 = \frac{1}{9}\left[\left(\frac{\partial \alpha_{xx}}{\partial \mathbf{Q}_p}\right)_0 + \left(\frac{\partial \alpha_{yy}}{\partial \mathbf{Q}_p}\right)_0 + \left(\frac{\partial \alpha_{zz}}{\partial \mathbf{Q}_p}\right)_0\right]^2 = \frac{1}{9}\sum_{\alpha\beta}\left(\frac{\partial \alpha_{\alpha\alpha}}{\partial \mathbf{Q}_p}\right)_0\left(\frac{\partial \alpha_{\beta\beta}}{\partial \mathbf{Q}_p}\right)_0 \tag{9}$$

$$\gamma_p^2 = \frac{1}{2}\sum_{\alpha\beta}\left[3\left(\frac{\partial \alpha_{\alpha\beta}}{\partial \mathbf{Q}_p}\right)_0^2 - \left(\frac{\partial \alpha_{\alpha\alpha}}{\partial \mathbf{Q}_p}\right)_0\left(\frac{\partial \alpha_{\beta\beta}}{\partial \mathbf{Q}_p}\right)_0\right] \tag{10}$$

Both the IR absorption and the Raman scattering factor of the p-th vibrational mode can be expressed as

$$I_p \propto \sum_l c_l \left(\frac{\partial P_l^{(1)}}{\partial \mathbf{Q}_p}\right)_0 \left(\frac{\partial P_l^{(2)}}{\partial \mathbf{Q}_p}\right)_0 \tag{11}$$

where $P_l^{(1)}$ and $P_l^{(2)}$ are components of the appropriate molecular property, that is, of the dipole moment vector $\boldsymbol{\mu}$ in the case of the IR absorption and of the electric dipole−electric dipole polarizability tensor α for the Raman scattering factor.

The total intensity of one band (i.e., the intensity integrated over the whole band), to which the k normal modes $\mathbf{Q}_p^{\mathrm{sub}}$ contribute, is given by

$$I^{\mathrm{band}} \propto \sum_{p=1}^{k}\sum_l c_l \left(\frac{\partial P_l^{(1)}}{\partial \mathbf{Q}_p^{\mathrm{sub}}}\right)_0 \left(\frac{\partial P_l^{(2)}}{\partial \mathbf{Q}_p^{\mathrm{sub}}}\right)_0 \tag{12}$$

As is shown in ref 18, this total intensity is invariant under unitary transformations among the contributing modes, and therefore the total intensities of the considered band can also be expressed in terms of the localized modes, that is

$$I^{\mathrm{band}} \propto \sum_{p=1}^{k}\sum_l c_l \left(\frac{\partial P_l^{(1)}}{\partial \tilde{\mathbf{Q}}_p^{\mathrm{sub}}}\right)_0 \left(\frac{\partial P_l^{(2)}}{\partial \tilde{\mathbf{Q}}_p^{\mathrm{sub}}}\right)_0 \tag{13}$$

This makes it possible to analyze the total intensity of the band under study in terms of the localized modes. Since the localized modes obtained for one band are in general rather similar, also the intensities with respect to the localized modes will be similar. Therefore, it will usually be sufficient to consider only one representative localized mode from this set in order to understand the effects that determine the total intensity of a certain band. One possibility for analyzing vibrational intensities is their decomposition into contributions of certain atoms or groups of atoms. Note that since only vibrations of a small number of atoms contribute to each localized mode, the localized modes simplify such an analysis considerably.

Finally we should mention that a scheme for the decomposition of the Raman and ROA invariants into local contributions of individual atoms or groups of atoms has been proposed by Hug,[20] which can be employed for analyzing the vibrational intensities with respect to the localized modes. Even though this analysis has only been applied to Raman and ROA invariants so far, also IR and VCD intensities can be decomposed in the same fashion. Since we will only consider IR and Raman spectroscopy here, we will only discuss the decomposition of the IR absorption and the Raman scattering factor in the following. Hug's decomposition scheme arises naturally when rewriting the property (i.e., dipole moment or polarizability) derivatives in terms of Cartesian displacements as

$$\left(\frac{\partial P_l}{\partial \tilde{\mathbf{Q}}_p}\right)_0 = \sum_A \left[\sum_{i\in A}\sum_{\alpha} \tilde{Q}_{i\alpha,p}^{(c)} \left(\frac{\partial P_l}{\partial R_{i\alpha}}\right)_0\right] \tag{14}$$

where A denotes appropriately chosen groups of atoms, in terms of which the decomposition is performed. For the IR absorption and the Raman scattering factor (as well as for the individual

Raman invariants), which are both given by a linear combination of products of property tensor derivatives, one obtains the local decomposition

$$I_p = \sum_l c_l \left(\frac{\partial P_l^{(1)}}{\partial \tilde{\mathbf{Q}}_p}\right)_0 \left(\frac{\partial P_l^{(2)}}{\partial \tilde{\mathbf{Q}}_p}\right)_0 = \sum_{AB} [J_p]_{AB} \qquad (15)$$

where I_p now stands for the IR absorption, Raman scattering factor, or one of the Raman invariants for which $P_l^{(1)}$ and $P_l^{(2)}$ are the required property tensor components and c_l the appropriate coefficients. The indices A and B run over the atoms or groups of atoms in terms of which the analysis is performed, and the local contributions are given by

$$[I_p]_{AB} = \sum_{i\in A,\ j\in B} \sum_{\alpha\beta} \tilde{Q}^{(c)}_{i\alpha,p} \tilde{Q}^{(c)}_{j\beta,p} \left[\sum_l c_l \left(\frac{\partial P_l^{(1)}}{\partial R_{i\alpha}}\right)_0 \left(\frac{\partial P_l^{(2)}}{\partial R_{j\beta}}\right)_0\right] \qquad (16)$$

While the diagonal terms $[I_p]_{AA}$ represent contributions that are solely due to the atoms in the group A, the off-diagonal terms $[I_p]_{AB}$ arise from the coupling between atoms in groups A and B. These local contributions can be visualized as group coupling matrices as proposed in ref 20 by representing the local contributions as circles with an area proportional to the size of the local contributions.

2.3. Analysis of Band Shapes in Terms of Localized Modes. While the total intensity of a band in the vibrational spectrum is invariant under a unitary transformation of the contributing normal modes, the intensities corresponding to the individual transformed modes differ from those of the normal modes. Therefore, in order to understand the shapes of the bands in the vibrational spectrum, the localized modes and their corresponding intensities alone are not sufficient, but also the couplings between them as well as the cross-terms in the intensities arising due to these couplings have to be considered.

In a similar fashion as described in the previous section for the decomposition into local contributions, IR and Raman intensities (as well as VCD and ROA intensities) of the normal modes within a certain band can be analyzed in terms of contributions of the corresponding localized modes. The normal mode $\mathbf{Q}_p^{\mathrm{sub}}$ can be expressed in terms of localized modes as[18]

$$\mathbf{Q}_p^{\mathrm{sub}} = \sum_q U_{qp}^T \tilde{\mathbf{Q}}_q^{\mathrm{sub}} = \sum_q U_{pq} \tilde{\mathbf{Q}}_q^{\mathrm{sub}} \qquad (17)$$

that is, the coefficients are given by the p-th column of $\mathbf{U}^T$, which can be obtained as an eigenvector of the coupling matrix $\tilde{\mathbf{\Omega}}$. Therefore, the intensity I_p associated with this mode can be decomposed as

$$I_p = \sum_{qr} [I_p]_{qr} = \sum_{qr} U_{pq} U_{pr} [I]_{qr} \qquad (18)$$

with the intensity coupling matrix

$$[I]_{qr} = \sum_l c_l \left(\frac{\partial P_l^{(1)}}{\partial \tilde{\mathbf{Q}}_q^{\mathrm{sub}}}\right)_0 \left(\frac{\partial P_l^{(2)}}{\partial \tilde{\mathbf{Q}}_r^{\mathrm{sub}}}\right)_0 \qquad (19)$$

This intensity coupling matrix describes the intensity and the arising coupling terms in terms of the localized modes, and the same intensity coupling matrix can be applied to all normal modes in the considered subset. Its diagonal elements $[I]_{qq}$ are given by the intensity with respect to the localized mode q, while the off-diagonal elements arise due to the coupling between two localized modes. Since the localized modes associated with one band in the vibrational spectrum are usually similar for modes located on different parts of the considered system, these terms will often show, similar to case of the coupling matrix $\tilde{\mathbf{\Omega}}$, a simple structure that is relatively easy to understand.

In order to obtain the decomposition of the intensity I_p with respect to a specific normal mode p in terms of localized modes according to eq 18, the elements of this intensity coupling matrix have to be multiplied by $U_{pq}U_{pr}$, that is, products of the coefficients of the localized modes that contribute to the normal mode p. These coefficients are determined by the vibrational coupling between the localized modes, that is, they are given by an eigenvector of the vibrational coupling matrix $\tilde{\mathbf{\Omega}}$.

If one considers the isotropic Raman invariant a^2 as the simplest case, the intensity coupling matrix is given by

$$[a]_{qr} = \left(\frac{\partial \bar{\alpha}}{\partial \tilde{\mathbf{Q}}_q^{\mathrm{sub}}}\right)_0 \left(\frac{\partial \bar{\alpha}}{\partial \tilde{\mathbf{Q}}_r^{\mathrm{sub}}}\right)_0 \qquad (20)$$

where $\bar{\alpha} = (1/3)(\alpha_{xx} + \alpha_{yy} + \alpha_{zz})$ is the isotropic polarizability. In general, the localized modes will be very similar, so that the derivatives of $\bar{\alpha}$ with respect to the localized modes will be almost identical and have the same sign if the phase of the localized modes is chosen in a consistent way. Therefore, all elements (diagonal and off-diagonal) will be positive and almost equal in size. With this in mind, one can easily see that the normal mode with the highest intensity is the mode in which all the prefactors $U_{pq}U_{pr}$ are positive, that is, the (nodeless) in-phase combination of the localized modes. At which vibrational frequency this highest-intensity normal mode occurs depends on the structure of the vibrational coupling matrix $\tilde{\mathbf{\Omega}}$ as well as on the vibrational frequencies of the localized modes.

However, in general the intensity coupling matrix will be more complicated and its structure will also depend on the orientation of the considered localized modes with respect to each other, so that other combinations of localized modes can turn out to lead to higher intensities. This is already true for the IR absorption, where a scalar product between the dipole moment derivatives with respect to the two localized modes has to be considered, and is further complicated in the case of VCD and ROA spectroscopy. Nevertheless, the decomposition analysis described above can be used to explain the intensity distribution within one band in the vibrational spectrum.

3. Computational Details

Structure optimizations were performed with the Turbomole program package[24,25] employing density-functional theory. The BP86 exchange-correlation functional[26,27] and Ahlrichs' valence triple-ζ basis with one set of polarization functions (TZVP) [28,29] and the corresponding auxiliary basis sets [30,31] were employed. All structures have been fully optimized. However, in order to converge to the desired local minima, constraints fixing the positions of different groups of atoms were applied in the initial phase of the optimization, but all these constraints were relaxed in the final stage of the optimization.

The program SNF[11,32] was used to calculate the normal modes and vibrational frequencies, as well as the dipole and polarizability derivatives that determine the IR absorption and the Raman scattering factor. As has been shown earlier by comparison to coupled-cluster calculations, DFT is able to reliably predict Raman scattering intensities.[33] The analytic energy gradients (needed for the seminumerical calculation of the harmonic force field) were calculated with Turbomole for distorted structures.[11,32] The Raman scattering factors were calculated for an excitation wavelength of 799 nm. It was verified that the chosen excitation wavelength is well away from any electronic absorption frequency of the considered molecules.

The calculations were performed for the isolated molecules and solvent effects were not included.

The localized modes were calculated according to the atomic-contribution criterion using the Jacobi-sweep method as described in ref 18. Both the localization of normal modes and the related analysis routines are implemented in an add-on package to SNF written in the Python programming language. The Numpy package[34] is used for efficient linear algebra operations where needed. For managing the geometric coordinates and for the assignment of atoms to individual residues and atom types in the investigated polypeptide, the Openbabel library[35,36] has been employed.

Pictures of molecular structures and normal modes were prepared with Jmol.[37] Plots of vibrational spectra and of group- and intensity-coupling matrices were produced using the Matplotlib package.[38] In the graphical representations of these coupling matrices, the area of the circles is proportional to the size of the corresponding matrix element, and filled circles represent positive whereas empty circles represent negative contributions. Note that for these symmetric matrices only the upper triangular part is shown, and the off-diagonal matrix elements have, therefore, been multiplied by two.

4. Results and Discussion

4.1. IR and Raman Spectra of α-Helical and 3_{10}-Helical $(Ala)_{20}$. In order to demonstrate how localized modes can be employed for analyzing how changes in the secondary structure affect the vibrational spectra, we study the calculated IR and Raman spectra of a polypeptide consisting of twenty (S)-alanine residues, denoted $(Ala)_{20}$, in an α-helical conformation and in a 3_{10}-helical conformation. Such a polypeptide can serve as a simple model for the vibrational spectrum of more complicated proteins and allows us to study how structural changes influence the amide bands in the IR and Raman spectra, which are commonly used to study protein structure.

The optimized structures of the polypeptides under investigation are shown in Figure 1. Note that the molecular structures of both polypeptides have been obtained from a full geometry optimization. Therefore, a rather large polypeptide containing twenty alanine residues has to be used in order to preserve the α-helical structure in the optimization. The structure of the α-helical $(Ala)_{20}$ polypeptide is identical to the one that was employed in ref 18. For the α-helix, the backbone dihedral angles of the central residues are approximately $\varphi = -60°$ and $\psi = -42°$, while for the 3_{10}-helix, they are approximately $\varphi = -63°$ and $\psi = -19°$ for the central residues, that is, the two conformers differ in the backbone dihedral angle ψ (the $C^{\alpha}C$ torsional angle), while φ (the NC^{α} torsional angle) is almost identical in both conformers. Note that at the termini, both helices are slightly distorted, and in the case of the α-helix, the termini tend to resemble a 3_{10}-helix. The Cartesian coordinates of both considered polypeptides are given in the Supporting Information.

The calculated IR and Raman spectra of α-helical and 3_{10}-helical $(Ala)_{20}$ in the region between 1800 and 1100 cm^{-1} are shown in Figure 2. In these spectra, the individual transitions, which are included as lines in the plotted spectra, have been broadened using a Lorentzian line shape with a half-width of 15 cm^{-1}. The first step toward the analysis of these vibrational spectra in terms of localized modes is the assignment of the individual vibrational transitions to certain bands in the spectrum. As described in ref 18, this assignment can be performed by considering the wavenumbers of the transitions, which for most vibrational bands cluster around the corresponding band maxima, and by collecting modes for which the contributions of certain groups of atoms to the normal modes show a similar pattern. The assignment of all modes within the considered wavenumber range can be found in the Supporting Information for both conformers of $(Ala)_{20}$.

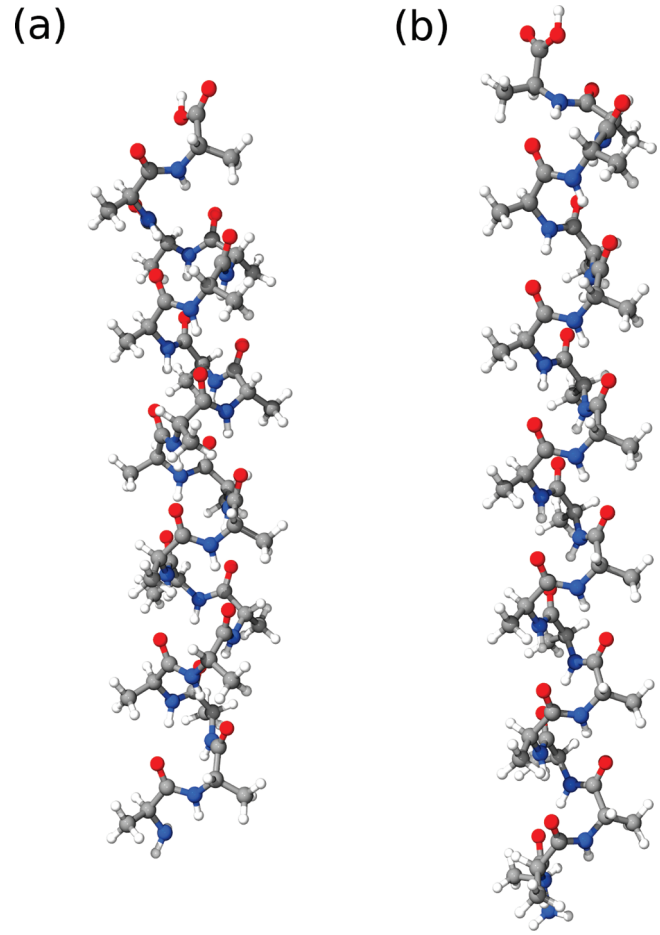

Figure 1. Optimized structures of $(Ala)_{20}$ in the conformation of (a) an α-helix and (b) a 3_{10}-helix.

All peaks in the IR and Raman spectra shown in Figure 2 can be assigned to one of these sets of normal modes. The wavenumber range of these sets of modes, the corresponding band maxima, as well as the calculated total IR absorption and Raman scattering factors of these bands are listed in Table 1 for the two $(Ala)_{20}$ conformations considered. The assignment of these groups of modes to certain types of vibrations has been discussed in detail in ref 18, where the displacements involved in each of these bands are visualized by considering the corresponding localized modes. The amide I modes are dominated by C═O stretching vibrations with smaller contributions of N−H bending and C^{α}−H bending vibrations. The amide II modes are due to the out-of-phase combination of the N−H bending and the C−N stretching vibrations of the amide group. The modes denoted as C^{α}−H bending and those denoted as amide III modes in Table 1 are usually jointly referred to as "extended amide III region", since all these modes consist of coupled N−H bending and C^{α}−H bending vibrations.[39] A detailed analysis of the bands in the extended amide III region and the coupling between N−H bending and C^{α}−H bending vibrations will be presented in Section 4.5.

Comparing the IR and Raman spectra calculated for the α-helical and the 3_{10}-helical conformation, one can identify a number of significant differences between the spectra. First,

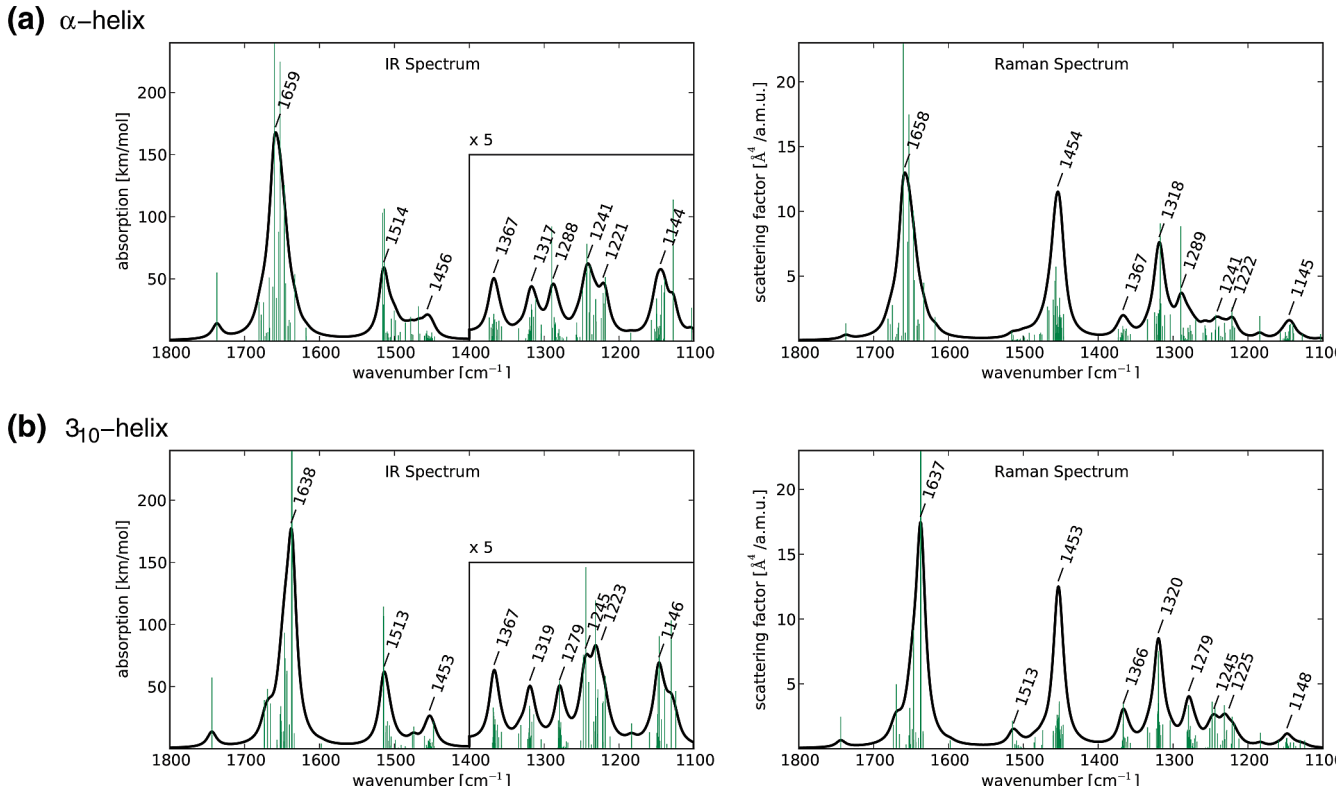

Figure 2. Calculated IR and Raman spectrum of (a) α-helical $(Ala)_{20}$ and (b) 3_{10}-helical $(Ala)_{20}$. The spectra have been plotted using a Lorentzian line width of 15 cm^{-1}. Individual peaks have been included as a line spectrum scaled by 0.2. In the IR spectrum, the region below 1400 cm^{-1} has been magnified by a factor of 5.

TABLE 1: Wavenumber Ranges, Band Maxima, and Sum of the IR Absorptions and Sum of the Raman Scattering Factors *S* for the Characteristic Bands in the Vibrational Spectra of α-Helical and 3_{10}-Helical $(Ala)_{20}$[a]

	range [cm^{-1}]	max [cm^{-1}]	total IR abs. [km/mol]	total Raman scattering factor [Å⁴/amu]
		α-helix		
amide I	1633−1681	1659	6279.9	483.1
amide II	1468−1515	1514	1918.6	30.3
$C^{\beta}H_3$ asymm bend	1446−1466	1456	496.4	322.8
$C^{\beta}H_3$ symm bend	1356−1373	1367	248.7	45.2
C^{α}−H bending (I)	1304−1334	1317	198.8	199.9
C^{α}−H bending (II)	1257−1290	1288	215.0	101.2
amide III	1184−1260	1221, 1241	528.4	95.8
skeletal C^{α}−N stretch	1103−1156	1144	353.6	47.5
		3_{10}-helix		
amide I	1631−1674	1638	5909.0	516.4
amide II	1474−1515	1513	1780.0	47.8
$C^{\beta}H_3$ asymm bend	1447−1457	1453	493.1	298.1
$C^{\beta}H_3$ symm bend	1357−1369	1367	295.2	67.3
C^{α}−H bending (I)	1304−1334	1319	231.9	215.3
C^{α}−H bending (II)	1268−1282	1279	213.4	92.6
amide III	1183−1259	1223, 1245	720.8	126.1
skeletal C^{α}−N stretch	1124−1159	1146	338.3	33.0

[a] Band maxima refer to the calculated IR spectrum.

while the amide II peak cannot be identified in the Raman spectrum of α-helical $(Ala)_{20}$, it is clearly visible for the 3_{10}-helix. This increased Raman scattering intensity can also be seen from the total scattering factors for the amide II modes given in Table 1, which increases from 30.3 Å⁴/amu for the α-helix to 47.8 Å⁴/amu for the 3_{10}-helix. Second, the position of the amide I peak shifts from 1659 to 1638 cm^{-1}, that is, by approximately 20 cm^{-1} when moving from an α-helix to a 3_{10}-helix. These two differences between the vibrational spectra will be investigated in detail in the following sections. Finally, even though the modes in the extended amide III region are usually believed to be very sensitive to structural changes, they are very similar for the α-helix and the 3_{10}-helix. Only the C^{α}−H bending (II) mode shifts by approximately 10 cm^{-1} from 1288 to 1279 cm^{-1}. To gain a better understanding of the structural factors determining the vibrational spectrum in the extended amide III region, these modes will be investigated in more detail in the following. But before proceeding to this investigation, it is worthwhile to compare the calculated vibrational spectra of the α-helical conformation to those observed in experiment.

TABLE 2: Comparison of the Band Maxima Calculated for $(Ala)_{20}$ to Those Measured in the Experimental IR Spectrum of α-(all-S)-Polyalanine[a]

	calc [cm^{-1}]	exp [cm^{-1}]
amide I	1659	1658
amide II	1514	1548
$C^{\beta}H_3$ asymm bend	1456	1461
$C^{\beta}H_3$ symm bend	1367	1384
C^{α}−H bending (I)	1317	1330
C^{α}−H bending (II)	1288	1305
amide III	1221, 1241	1274
skeletal C^{α}−N stretch	1144	1168

[a] Experimental values are taken from ref 42.

4.2. Comparison to the Experimental Spectrum of α-Helical Polyalanine. In experiments performed in aqueous solution, such $(Ala)_{20}$ polypeptides do not adopt the nearly ideal α-helical structure investigated here computationally but are instead frayed at the termini, and their structure is very sensitive to temperature due to this (partial) unfolding.[40] Therefore, we compare to the experimental spectrum of solid (all-S)-polyalanine,[41,42] which adopts an α-helical conformation. The calculated IR band maxima as well as those observed in the experimental IR spectrum for the considered wavenumber range are given in Table 2. Note that for the 3_{10}-helical conformation, no direct comparison to experimental data is possible since this conformation is in general not observed for alanine polypeptides, but $C^{\alpha,\alpha}$-disubstituted residues are required to support a 3_{10}-helical conformation in short polypeptides.[43] However, this is no drawback in our computational experiment, which only requires both helical structures to be a local minima on the potential energy surface.

The comparison shows an excellent agreement of the calculated band maxima to those observed in experiment for the amide I and the side chain $C^{\beta}H_3$ bending modes with an error smaller than 10 cm^{-1}. However, this good agreement is partially due to a fortunate error cancelation,[23,44–47] since one would expect that the harmonic approximation, the deficiencies of the approximate exchange-correlation functional employed in the DFT calculations, and the neglect of solvent and bulk effects lead to deviations of the calculated band maxima from those observed in experiment. For the amide II modes, the extended amide III region, and the skeletal stretch band the experimental wavenumbers are underestimated by up to 30 cm^{-1}. These modes all involve some contribution of N−H bending vibrations that can be expected to be most sensitive to solvent effects that were neglected in our calculations.

It should be noted that in previous DFT calculations on α-helical alanine polypeptides, larger deviations between the experimentally observed amide I IR bands and the calculated ones, which appeared at approximately 1720 cm^{-1}, were found.[48] This was attributed to the absence of solvent effects, and it was shown that the inclusion of explicit water solvent molecules shifts the calculated amide I band to approximately 1670 cm^{-1}. While solvent effect will certainly affect the amide bands significantly, there are also a number of other sources of errors in the calculations of ref 48 that can account for the observed large shift of the amide I band. In particular, the vibrational spectra were simulated by transferring force constants calculated for smaller fragments to the large system,[49] which only partly includes the environment of the individual residues in the polypeptide and neglects the coupling between different residues. Furthermore, an idealized α-helical conformation was used for the small alanine oligopeptides in ref 48 from which the force constants were obtained, and the backbone dihedral angles were constrained during the structure optimization. Therefore, the effect of the intramolecular hydrogen bonds that significantly affects the electronic structure of the amide group will only be described partially.

The simplest way to include the effect of a solvent environment in the calculations is to employ a continuum solvation model.[50,51] Note that such a continuum solvation model cannot be expected to yield an accurate description of specific solvent effects (i.e., of hydrogen bonds between solvent molecules and the solute), and therefore it can only be considered as a first estimate. To test the significance of continuum solvation effects for the calculated vibrational spectra, we performed calculations employing the conductor-like screening model (COSMO).[52] Details on these calculations as well as the IR and Raman spectra calculated using the COSMO model can be found in the Supporting Information. However, as is discussed there, including continuum solvation effects changes neither the molecular structures nor the vibrational spectra significantly. In both the IR and the Raman spectra, the positions and intensities of the bands within the considered wavenumber range only change slightly (the shifts in the band maxima are 20 to 30 cm^{-1} for the amide I band and less than 10 cm^{-1} for all other bands) and all the qualitative features of the spectra that will be discussed in the following are preserved. This shows that in order to describe the effects of the solvent or bulk environment more accurately, more sophisticated solvent models that explicitly include the molecular structure of the environment would be required (see, e.g., ref 48 for the description of solvent effects on vibrational spectra, and refs 53–55 and references therein for other molecular properties). For our purposes here, it will be sufficient not to include continuum solvent effects in the following.

4.3. Decomposition of the Raman Intensity of the Amide II Band. The amide II modes in polypeptides and proteins, which are mainly due to an out-of-phase combination of N−H bending and C−N stretching vibrations of the amide groups, are very prominent peaks in IR and VCD spectra, that have been used extensively for investigations of secondary structure.[4,56] In the Raman spectrum, the amide II band is generally weak or absent.[39] However, it can be prominent in the ultraviolet (UV) resonance Raman spectrum[57] and also in ROA spectra, where they provide useful information on protein conformation.[6,58]

In the calculated Raman spectra of $(Ala)_{20}$, the amide II band is only found in the spectrum of the 3_{10}-helical conformation, while it is too weak to be visible in the spectrum of the α-helical conformation. To understand the Raman intensity of the amide II band, which is the sum of the intensities of a number of delocalized amide II normal modes, it is instructive to look at the corresponding localized modes. These will show a more regular intensity pattern, that is, all localized modes will exhibit a very similar intensity, though all intensities still sum up to the same total intensity. Therefore, it is sufficient to investigate only one of these localized modes in more detail.

We will consider the localized mode which features the bending of N−H of residue 12 as a main contribution. This localized mode is shown in Figure 3a, and it can be seen that it is almost identical for the two conformers. However, while for the α-helix the considered localized mode has a scattering factor of 0.95 $Å^4$/amu, it increases to 2.05 $Å^4$/amu for the 3_{10}-helix. Therefore, this localized mode reflects the observed increase of the total scattering intensity of the amide II band.

To analyze the Raman scattering factor associated with the considered localized mode, the Raman scattering factor can be

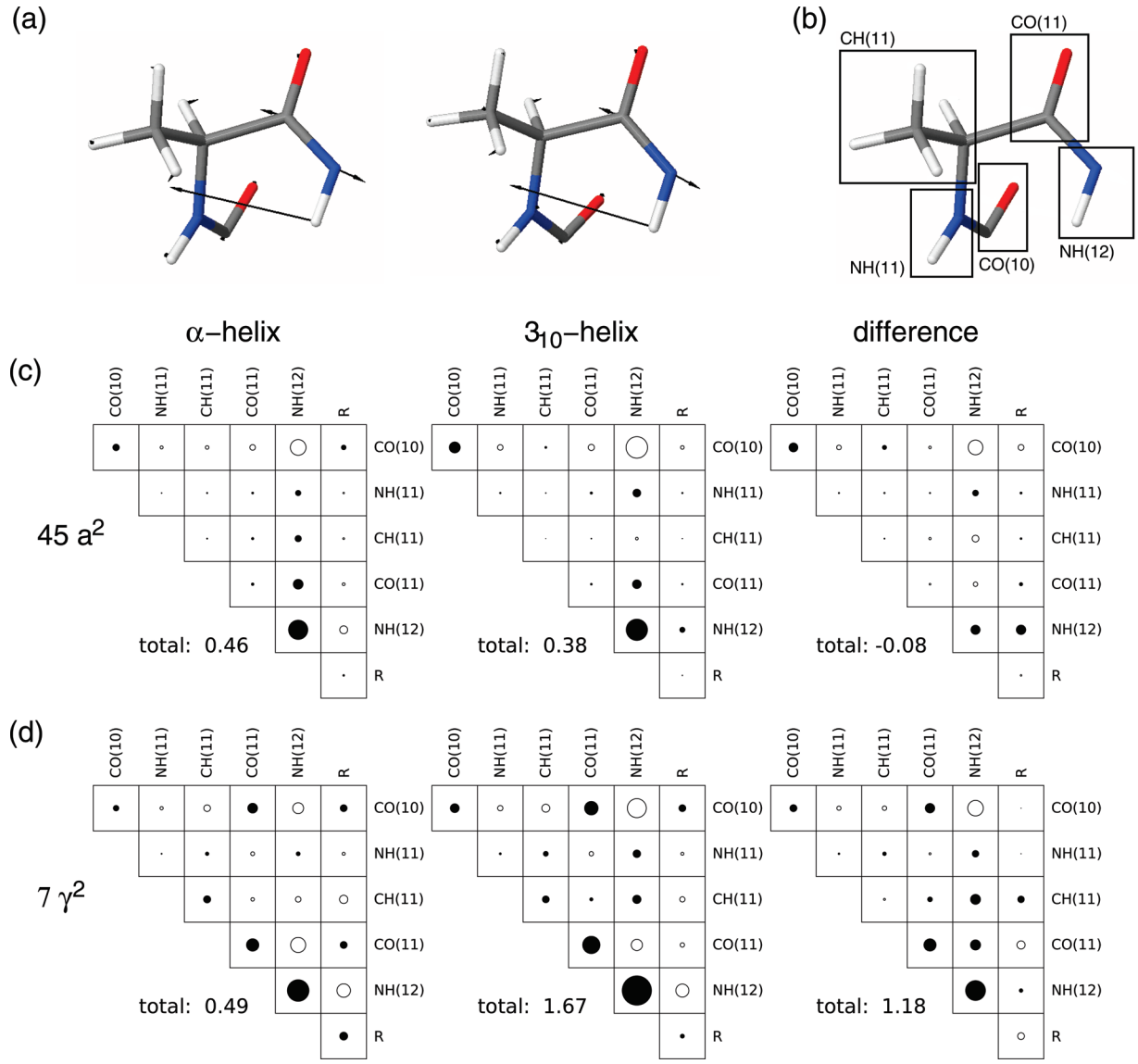

Figure 3. Analysis of the amide II Raman intensity. (a) Localized amide II mode with the main contribution on the N−H group of residue 12. Only the atoms of residue 11 and the adjacent N−H and C═O groups are shown. The contributions of all other atoms to this mode are negligible. (b) Groups of atoms that are used for the decomposition into group contributions. All other atoms are collected in the group labeled "R". (c) Group coupling matrices showing the decomposition of the isotropic Raman invariant $45a^2$ for $(Ala)_{20}$ in the conformation of an α-helix (left) and of a 3_{10}-helix (middle), and difference between the two conformations (right). In all three cases, also the total value of $45a^2$ (in Å^4/amu) is given. (d) Group coupling matrices showing the analogous decomposition of the anisotropic Raman invariant $7\gamma^2$. In all three cases, also the total value of $7\gamma^2$ (in Å^4/amu) is given.

decomposed into contributions of groups of atoms as described in Section 2.2. For this decomposition, we will consider the isotropic and anisotropic Raman invariants $45a^2$ and $7\gamma^2$ separately. The coefficients in front of these invariants are included so that their total values are comparable. The Raman invariants are decomposed into contributions of the N−H, of the C═O group, of the C^{α}−H, and of the $C^{\beta}H_3$ groups of residue 11, as well as of the adjacent C═O and N−H groups of residues 10 and 12, respectively, and those of all other atoms (labeled "R"). These groups are shown in Figure 3b.

The decomposition of the isotropic Raman invariant $45a^2$ is shown in Figure 3c. The main contribution is for both conformations the one of the N−H group of residue 12, which could be expected since this group also has the largest contribution to the mode under investigation. However, the contributions are almost identical for both conformations, and the difference between the $45a^2$ invariant for the two conformations is close to zero, that is, the observed increase in the Raman scattering factor is not caused by an increase of the isotropic invariant $45a^2$, but is due to the anisotropic invariant $7\gamma^2$.

The decomposition of the anisotropic Raman invariant $7\gamma^2$ is shown in Figure 3d. As for $45a^2$, the largest contribution is due to the N−H group of residue 12, but there is also a significant contribution from the adjacent C═O group of residue 11 and, to a smaller extent, from the C═O group of residue 10. However, the anisotropic invariant $7\gamma^2$ is different for the α-helical and the 3_{10}-helical conformations, and the group coupling matrices in Figure 3 show that this difference is almost exclusively due to the diagonal terms associated with the N−H group of residue 12 and the C═O group of residue 11, that is, the differences can be associated with the C−N stretching vibration. Since the localized mode under investigation is almost identical for both conformations, these differences must be due to variations in the derivatives of the anisotropy of the polarizability that are caused by the changes in the electronic structure induced by the different molecular structures. Note

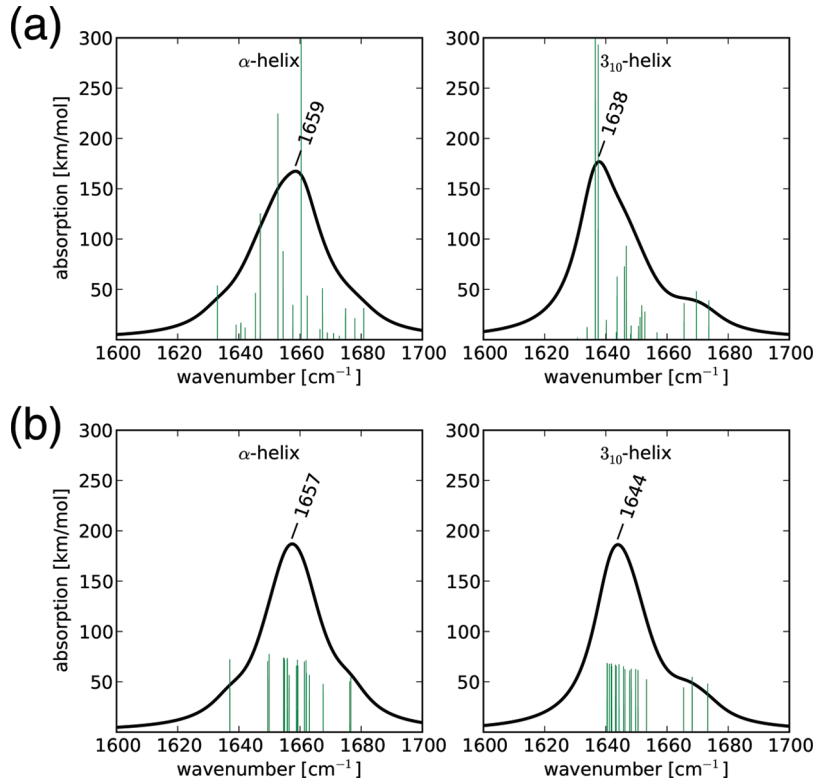

Figure 4. (a) Amide I band in the calculated IR spectrum of α-helical (left) and 3_{10}-helical (right) $(Ala)_{20}$. The individual transitions are included as a line spectrum scaled by 0.2. (b) Amide I band in the fictitious IR spectra defined in terms of localized modes. The contributions of the individual localized modes are included as a line spectrum scaled by 0.2.

that the increased Raman intensity is not caused by an increased coupling of the amide II modes with the very intense $C^{\beta}H_3$ bending modes, as could be expected at first sight.

4.4. Understanding the Frequency Shift of the Amide I Band. In our calculated IR spectra, the maximum of the amide I band is shifted to lower wavenumbers from 1659 cm^{-1} for α-helical $(Ala)_{20}$ to 1638 cm^{-1} for the 3_{10}-helical conformation, that is, by 21 cm^{-1}. In this section, we analyze the origin of this shift. We note that a similar shift of the amide I peak to lower wavenumbers between an α-helical and a 3_{10}-helical alanine polypeptide was obtained previously in the calculations of Keiderling and co-workers.[8] However, they also found that this shift is counteracted by the α-methyl substitution in the $C^{\alpha,\alpha}$-disubstituted model peptides adopting a 3_{10}-helical conformation that they also investigated experimentally, so that this shift cannot be employed to distinguish the two conformations experimentally.

The amide I band in the calculated IR spectrum for the α-helix and the 3_{10}-helix are shown in Figure 4a, where also the underlying vibrational transitions are included as a line spectrum. It can be seen that the band maxima are in both cases due to only a few very intense transitions. When considering the corresponding localized modes, the picture changes and all localized modes exhibit very similar intensities, and also show quite similar wavenumbers. This can be seen in the fictitious spectra in terms of localized modes, which are shown in Figure 4b. These spectra are obtained by plotting the IR spectrum one would obtain if the localized modes were the true normal modes (i.e., if the coupling between them could be neglected).

In these fictitious spectra in terms of localized modes, the maxima of the amide I band occur at 1657 and 1644 cm^{-1} for the α-helix and the 3_{10}-helix, respectively. The difference of 13 cm^{-1} between the maxima found for the two conformations is due to the shift in the vibrational frequencies of the localized modes. Therefore, this shift is caused by changes of the force constants that are due to the conformational change, that is, differences in the local electronic structure of the carbonyl groups. However, this shift only accounts for a part of the shift of 21 cm^{-1} found in the true spectrum.

To explain the remaining shift, one has to consider the coupling between the localized amide I modes on different residues. It is well known that the shape and position of the amide I band in polypeptides and proteins is largely influenced by the coupling between the individual carbonyl stretching vibrations. This was first recognized by Krimm and co-workers, who showed that the splitting of the amide I band in β-sheet polypeptides can be explained by using a simple dipole coupling model.[59,60] Such empirical transition dipole coupling (TDC) constants have since then been used in numerous theoretical studies.[41,61,62] However, the TDC model neglects the effects of through-bond coupling, and it has been shown that for residues that are close to each other, the TDC model leads to significant deviations of the resulting vibrational frequencies.[63,64] In contrast, our approach allows it to extract coupling constants from full quantum chemical calculations, that include all these effects and that do not rely on any empirical models. As was shown in ref 18, the TDC model is able to qualitatively reproduce these full coupling constants only for the amide I band (even though the magnitudes of the TDC coupling constants deviate significantly), while for all other bands, the TDC coupling constants are even qualitatively wrong.

In order to simplify the analysis, we will only consider the six localized modes with their main contributions on residues 7 to 12. For the localized modes at the terminal residues, the vibrational frequencies are shifted, which would further complicates the observed coupling patterns. However, the restricted

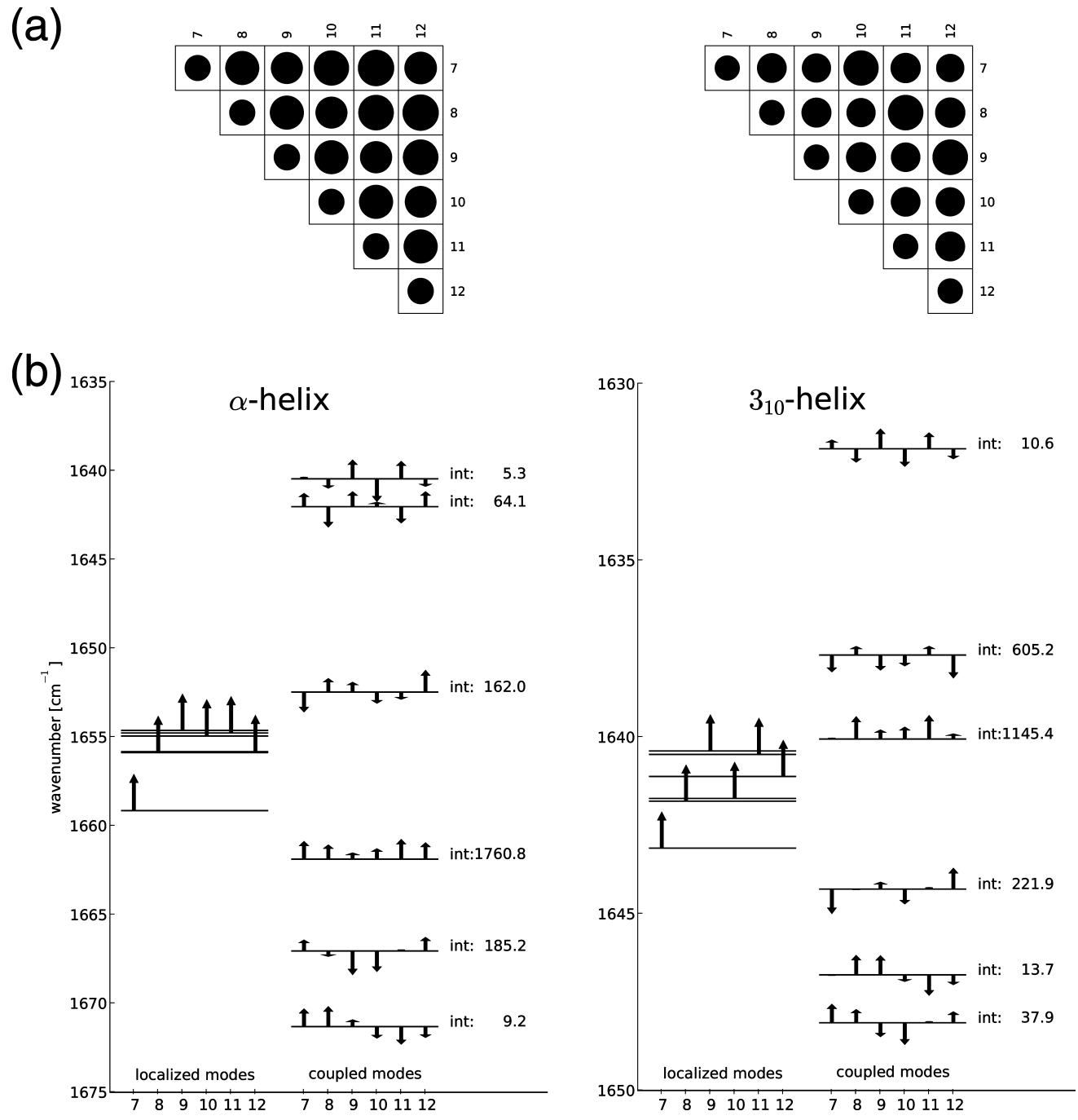

Figure 5. (a) Intensity coupling matrices for the localized amide I modes on residues 7 to 12 of α-helical (left) and of 3_{10}-helical (right) $(Ala)_{20}$. (b) Graphical representation of the considered localized modes (left column of each plot) and the corresponding coupled modes, that is, eigenvectors of the considered subblock of the coupling matrix $\tilde{\mathbf{\Omega}}$ (right column of each plot) for the two considered conformations. The positions of the lines indicate the wavenumbers of the localized modes and the coupled modes, respectively. For each mode, the arrows indicate its composition by giving the coefficients of the contributing localized modes. The values labeled "int" are the IR absorptions in km/mol corresponding to the coupled mode.

subset of six localized modes already allows for a qualitative understanding.

As discussed in Section 2.2, the distribution of the intensity across the normal modes in one band of the spectrum is determined by the intensity coupling matrix, $[\boldsymbol{\mu}^2]_{qr}$ in the case of the IR intensity, and by the coefficients of the normal modes with respect to the localized modes, which are determined by the vibrational coupling matrix $\tilde{\mathbf{\Omega}}$. Graphical representations of the IR intensity coupling matrices for the considered subset of localized modes of α-helical and 3_{10}-helical $(Ala)_{20}$ are shown in Figure 5a. These matrices show a rather simple pattern. All off-diagonal elements, which describe the coupling terms in the IR intensity between the localized modes, are positive and of similar size. The small differences between the elements corresponding to a different distance between the residues (i.e., the different secondary diagonals of the matrices in Figure 5a) are due to the slight differences in the orientation of the corresponding transition dipole vectors.

Since all the off-diagonal elements of the IR intensity coupling matrices are positive, the normal mode with the highest intensity will be the in-phase combination of the localized modes, that is, the normal mode in which all the coefficients

TABLE 3: Subblock of the Amide I Coupling Matrices $\tilde{\Omega}$ Corresponding to the Localized Modes on Residues 7 to 12 for $(Ala)_{20}$ in the Conformation of an α-Helix and of a 3_{10}-Helix[a]

α-helix	7	8	9	10	11	12
7	1659.1	8.5	–2.2	–4.2	–0.4	–0.5
8	8.5	1655.9	7.9	–2.3	–4.2	–0.4
9	–2.2	7.9	1654.6	8.2	–2.2	–4.4
10	–4.2	–2.3	8.2	1654.9	8.3	–2.1
11	–0.4	–4.2	–2.2	8.3	1654.8	8.2
12	–0.5	–0.4	–4.4	–2.1	8.2	1655.8
3_{10}-helix	7	8	9	10	11	12
7	1643.1	2.5	–3.7	–0.7	–0.6	–0.6
8	2.5	1641.8	2.7	–3.7	–0.8	–0.6
9	–3.7	2.7	1640.4	2.8	–3.8	–0.8
10	–0.7	–3.7	2.8	1641.7	2.4	–3.7
11	–0.6	–0.8	–3.8	2.4	1640.5	2.5
12	–0.6	–0.6	–0.8	–3.7	2.5	1641.1

[a] The phase of the localized modes is chosen such that all nearest-neighbor coupling constants $\tilde{\Omega}_{i,i+1}$ are positive. All values in cm^{-1}.

with respect to the localized modes have the same sign. The vibrational frequencies and the composition of the normal modes considered in terms of localized modes are obtained as eigenvalues and eigenvectors of the vibrational coupling matrix $\tilde{\mathbf{\Omega}}$, respectively. Table 3 shows the subblock of $\tilde{\mathbf{\Omega}}$ corresponding to the localized amide I modes with their major contribution of residues 7 to 10 for the two conformations of $(Ala)_{20}$ under study here.

As expected, in both cases one finds that the elements on one diagonal, which correspond to the same distance between residues, are rather similar. For the α-helix, the largest couplings occur between nearest-neighbor residues, with coupling constants of $\tilde{\Omega}_{i,i+1} \approx 8.2$ cm^{-1}. For residues that are further apart, the coupling constants are negative. For the second nearest-neighbor, the coupling constant is with $\tilde{\Omega}_{i,i+2} \approx -2.2$ cm^{-1} smaller as for the nearest neighbor, and a somewhat larger coupling constant of $\tilde{\Omega}_{i,i+3} \approx -4.3$ cm^{-1} is found for the third nearest-neighbor, which corresponds to one complete turn of the α-helix. For residues that are even further apart, the magnitude of the coupling constants is smaller than 1 cm^{-1}. For the 3_{10}-helix, a different pattern is found. The nearest-neighbor coupling constants are with $\tilde{\Omega}_{i,i+1} \approx 2.6$ cm^{-1} smaller than in the α-helix case. The second nearest-neighbor coupling constants of $\tilde{\Omega}_{i,i+2} \approx -3.7$ cm^{-1}, which now corresponds to one complete turn of the 3_{10}-helix, are even larger in magnitude. The magnitude of the coupling constants between residues that are further apart are smaller than 1 cm^{-1}.

These different coupling patterns lead to different normal modes and to a different vibrational frequency of the most intense mode, that is, of the in-phase combination of localized modes. To illustrate this, a graphical representation of the resulting coupled modes (i.e., eigenvectors of the subblock of the considered coupling matrix $\tilde{\mathbf{\Omega}}$) as well as the corresponding eigenvalues are shown in Figure 5b. Note that since only a subblock of $\tilde{\mathbf{\Omega}}$ is considered, these eigenvectors do not correspond to the true normal modes (which could be obtained from the full coupling matrix). Nevertheless, these eigenvectors demonstrate the influence of the different coupling patterns on the resulting eigenvectors, which can also be found for the eigenvectors of the full coupling matrix. For the α-helix, where the largest coupling constants occur between nearest-neighbor residues, the in-phase combination appears at approximately 1662 cm^{-1}, that is, shifted to higher wavenumbers with respect to the localized modes. In contrast, for the 3_{10}-helix, where the second nearest-neighbor coupling constants are larger than the nearest-neighbor ones, the in-phase combination appears at approximately 1640 cm^{-1}, that is, shifted to lower wavenumbers with respect to the localized modes.

About 13 cm^{-1} of the total shift of the amide I peak between the α-helix and the 3_{10}-helix could be explained by a shift of the vibrational frequencies of the localized modes. The remaining shift of about 8 cm^{-1} can be attributed to the different structure of the coupling matrix $\tilde{\mathbf{\Omega}}$. While in the case of the α-helix, the coupled mode with the highest intensity appears at higher wavenumbers than the localized modes, as in the case of the 3_{10}-helix the coupled mode with the highest intensity at lower wavenumbers than the localized modes. By employing an analysis in terms of localized modes, it is possible to separate these two contributions to the shift of the vibrational frequency and to further analyze both contributions.

4.5. Analysis of the Bands in the Extended Amide III Region. The extended amide III region of the vibrational spectra of polypeptides and proteins approximately comprises the wavenumber range between 1200 and 1350−1400 cm^{-1}. In this region, a number of bands appear that are due to the coupling of the "classical amide III" mode, which is an in-phase combination of the N−H bending and the C−N stretching vibration of the amide group, with the C^{α}−H bending vibrations. Because of this coupling, these modes in the extended amide III region are particularly sensitive to changes in the secondary structure,[65,39,66] which has been explored in a number of experimental and theoretical studies attempting to exploit this sensitivity for the determination of protein structure using vibrational spectroscopy.[57,67–69] Mostly, the bands in the extended amide III region are measured in Raman and in UV resonance Raman spectroscopy, which enhances these backbone vibrations.

Nevertheless, the understanding of how the secondary structure determines the vibrational frequencies of the bands in the extended amide III region still remains rather incomplete. Most of the knowledge concerning the origin of the bands in the extended amide III region comes from experimental and theoretical investigations performed for di- or tripeptides. In two pioneering studies,[70,71] which still form the basis for most discussions of the extended amide III region in polypeptides and proteins, Diem and co-workers measured the IR and Raman spectra of various isotopomers of (S,S)-alanylalanine. They find that the classical amide III mode, which can be observed in the isotopomer deuteriated at both C^{α} positions, appears at 1336 cm^{-1}. The C^{α}−H bending modes of the C-terminal residue appear at 1330 and 1279 cm^{-1}, while those of the N-terminal residue are found at 1355 and 1305 cm^{-1}. In the nondeuteriated isotopomer, these five modes strongly couple to a set of normal

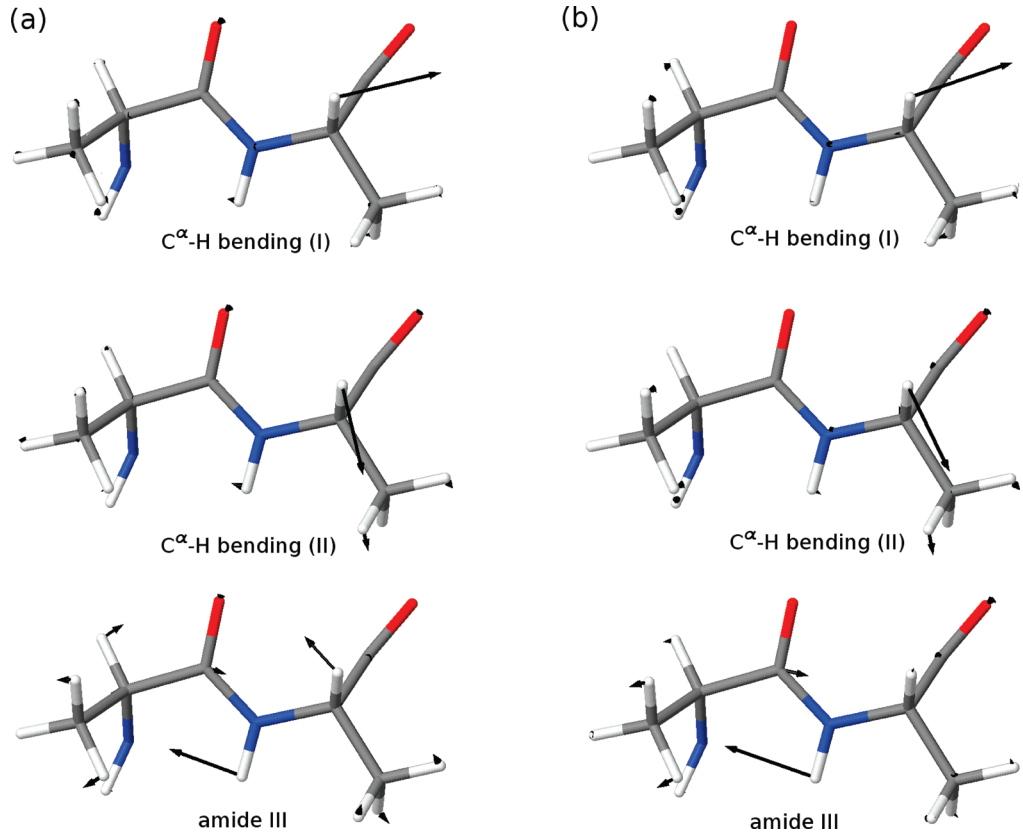

Figure 6. Localized modes for the extended amide III region of α-helical $(Ala)_{20}$ obtained by performing the localization (a) for the subsets of normal modes in each of the three bands individually (band-localized modes) and (b) for the subset of all normal modes within the three bands at once (region-localized modes). Only residues 9 and 10 are shown, the remaining parts of the helix are left out for clarity. For each set of localized modes, only the modes with the largest contribution on residue 10 are shown.

modes that are combinations of the classical amide III mode and $C^{\alpha}-H$ bending vibrations.

However, one has to realize that while for this small dipeptide the two $C^{\alpha}-H$ groups are very different (with differences in the $C^{\alpha}-H$ bending frequencies of approximately 25 cm^{-1}), in larger polypeptide or proteins the $C^{\alpha}-H$ groups on both sides of the amide group are in general in a very similar environment and, therefore, can be expected to have similar vibrational frequencies. This will significantly affect the coupling between $C^{\alpha}-H$ bending and N−H bending modes and thus also change the resulting vibrational frequencies. Therefore, studies investigating the structural dependence of the amide III bands for di- or tripeptides (see, e.g., refs 72 and 73) in many cases cannot be employed directly to extrapolate to larger polypeptides and proteins.

Therefore, calculations on larger polypeptides are mandatory in order to investigate the structural dependence of the bands in the amide III region, and an analysis in terms of localized modes can be employed to gain an understanding of the factors determining the observed bands. In our calculated spectra, for α-helical and 3_{10}-helical $(Ala)_{20}$, three distinct bands in the extended amide III region can be identified, which in Table 1 have been designated as $C^{\alpha}-H$ bending (I), $C^{\alpha}-H$ bending (II), and amide III.

In order to gain a better understanding of the origin of these bands, we transform the normal modes within each of these band to localized modes. Since the localization procedure is applied to each of the three bands separately, these modes will be referred to as band-localized modes. The localized modes with their main contribution on residue 10 are visualized in Figure 6a as representative examples of the localized modes corresponding to the three bands. Since only a very limited number of atoms contributes to these localized modes the visualization of these modes is greatly simplified, and it is sufficient to only show the atom of residues 9 and 10, since the contributions of all other atoms are negligible.

As Figure 6a shows, the $C^{\alpha}-H$ bending (I) modes are mainly due to a vibration of the $C^{\alpha}-H$ group along the direction of the $N-C^{\alpha}$ bond, while the $C^{\alpha}-H$ bending (II) mode is due to a vibration of the $C^{\alpha}-H$ group that is approximately perpendicular to the $N-C^{\alpha}$ bond. In both cases, also smaller contributions of an N−H bending vibration and of an asymmetric $C^{\beta}H_3$ bending vibration are present. The modes designated as amide III are mainly due to the classical amide III vibration, that is, an in-phase combination of the N−H bending and C−N stretching vibrations of the amide group. However, it also shows large contributions of a $C^{\alpha}-H$ bending vibration which is approximately perpendicular to the $N-C^{\alpha}$ bond and of an asymmetric $C^{\beta}H_3$ bending vibration. We note that this assignment is consistent with the experimental IR and Raman spectra of (all-S)-polyalanine given in ref 42, where also three bands are observed in the extended amide III region. Upon deuteriation of the N−H groups, the two bands at higher wavenumbers (i.e., those that are mainly due to $C^{\alpha}-H$ bending) only shift slightly by less than 10 cm^{-1}, while the band at lower wavenumber (i.e., the classical amide III band) shifts outside the extended amide III region.

However, one distinct feature of our calculated spectra that does not agree with the experimental spectra of polyalanine are the two maxima that are found for the amide III band. These

TABLE 4: Subblock of the Extended Amide III Coupling Matrices $\tilde{\Omega}$ Corresponding to the Region-Localized Modes on Residues 9 and 10 of α-Helical and 3_{10}-Helical $(Ala)_{20}$[a]

		α-helix					
		9			10		
		AmIII	$C^{\alpha}H$ (I)	$C^{\alpha}H$ (II)	AmIII	$C^{\alpha}H$ (I)	$C^{\alpha}H$ (II)
9	AmIII	1255.1	12.2	15.5	–7.5	0.5	–0.9
	$C^{\alpha}H$ (I)	12.2	1315.2	3.9	–7.8	0.9	–0.1
	$C^{\alpha}H$ (II)	15.5	3.9	1276.1	11.6	–0.6	0.0
10	AmIII	–7.5	–7.8	11.6	1256.5	11.8	15.2
	$C^{\alpha}H$ (I)	0.5	0.9	–0.6	11.8	1315.8	3.8
	$C^{\alpha}H$ (II)	–0.9	–0.1	0.0	15.2	3.8	1275.4
		3_{10}-helix					
		9			10		
		AmIII	$C^{\alpha}H$ (I)	$C^{\alpha}H$ (II)	AmIII	$C^{\alpha}H$ (I)	$C^{\alpha}H$ (II)
9	AmIII	1254.3	11.7	16.6	–6.6	0.2	–1.0
	$C^{\alpha}H$(I)	11.7	1316.2	5.4	–4.1	1.2	0.0
	$C^{\alpha}H$(II)	16.6	5.4	1271.3	8.1	–0.3	0.1
10	AmIII	–6.6	–4.1	8.1	1254.0	11.4	16.7
	$C^{\alpha}H$(I)	0.2	1.2	–0.3	11.4	1314.4	5.9
	$C^{\alpha}H$(II)	–1.0	0.0	0.1	16.7	5.9	1270.7

[a] "$C^{\alpha}H$ (I)" and "$C^{\alpha}H$ (II)" refer to the two $C^{\alpha}-H$ bending modes, while "AmIII" is used for the classical amide III mode. The phase of the region-localized modes is chosen as shown in Fig. 6b. All values in cm^{-1}.

appear in the IR spectra at 1241 and 1221 cm^{-1} for the α-helix and at 1245 and 1223 cm^{-1} for the 3_{10}-helix. This can be understood by considering the vibrational frequencies of the localized modes obtained for the amide III band. While for the central residues, these are in the range between 1235 to 1250 cm^{-1}, those of the terminal residues are shifted to significantly lower wavenumbers and appear between 1200 and 1230 cm^{-1}. Therefore, the maxima at 1221 and 1223 cm^{-1}, respectively, are due to the terminal residues. For these residues the frequencies of the localized amide III modes are significantly lower, since at the termini the amide groups are only involved in one hydrogen bond while for the central residues they are involved in two hydrogen bonds. For the amide III band, this different hydrogen bonding has a much larger effect than for the $C^{\alpha}-H$ bending modes, where the shift of the frequencies of the localized modes on the terminal residues is with only about 10 cm^{-1} much smaller.

To obtain a more detailed picture of the coupling between the $C^{\alpha}-H$ bending and the amide III vibrations, it is beneficial to consider another set of localized modes. Instead of performing the localization for each of the three bands in the extended amide III region separately, which leads to the band-localized modes discussed above, one can also perform the localization for all normal modes within the extended amide III region. The resulting localized modes will be referred to as region-localized modes. Similar to the band-localized modes, the region-localized modes on different residues are very similar, and for each residue one finds three different region-localized modes with their main contribution on this residue.

As a representative example, the three region-localized modes with the main contribution on residue 10 are shown in Figure 6b. As can be seen, the region-localized modes differ from the band-localized modes. While for the latter, the $C^{\alpha}-H$ bending and the classical amide III vibration are mixed, for the region-localized modes one obtains two almost pure $C^{\alpha}-H$ bending modes (one in which the bending vibration is along the $N-C^{\alpha}$ bond and one in which it is perpendicular to the $N-C^{\alpha}$ bond) and one almost pure amide III mode (i.e., an in-phase combination of the N−H bending and the C−N stretching vibration).

The coupling between the pure $C^{\alpha}-H$ bending and amide III modes can now be analyzed by considering the coupling matrix $\tilde{\Omega}$ with respect to the region-localized modes. The subblock of $\tilde{\Omega}$ corresponding to the modes on residues 9 and 10 is given in Table 4 for both the α-helical and the 3_{10}-helical conformation of $(Ala)_{20}$. Note that in this Table the localized modes on each residue are not ordered according to their vibrational frequency but according to the order in which the involved groups of atoms appear in the polypeptide.

The different coupling constants are affected by the change in secondary structure between the two considered conformers in different ways. For the coupling between the amide III mode and the $C^{\alpha}-H$ bending modes on the same residue one finds coupling constants of approximately 12 cm^{-1} and approximately 16 cm^{-1} for both the α-helix and for the 3_{10}-helix. The orientation between the groups involved in this vibration (the amide group and the $C^{\alpha}-H$ group of the same residue) is determined by the backbone dihedral angle φ (i.e., the $N-C^{\alpha}$ torsional angle). This torsional angle is very similar for both structures, which explains the almost identical coupling constants. In contrast to this, for the coupling between the amide III mode on residue 10 with the $C^{\alpha}-H$ bending modes on residue 9, the coupling constants differ for the two conformers. While coupling constants of −7.8 and 11.6 cm^{-1} are found for the α-helical conformation, the corresponding coupling constants are −4.1 and 8.1 cm^{-1} in the 3_{10}-helix. For these coupling constants, the orientation between the involved groups, the $C^{\alpha}-H$ of residue 9 and the amide group connecting residues 9 and 10, is determined by the backbone dihedral angle ψ, which differs in the two conformers. This change is reflected by the change in the coupling constants. For the coupling between the amide III mode of residue 9 and the $C^{\alpha}-H$ bending modes on residue 10, the coupling constants are smaller than 2 cm^{-1}, which can be understood since the groups involved in these vibrations are further apart. Similarly, the coupling constants between localized modes on residues which are further apart (i.e., those couplings not shown in Table 4) are generally smaller than 2 cm^{-1}.

In addition to the differences in the coupling constants, also the changes in the vibrational frequencies of the localized modes (i.e., the diagonal elements of the coupling matrix shown in Table 4) have to be considered. While the wavenumbers of the region-localized amide III and $C^{\alpha}-H$ bending (I) modes are very similar for both conformations, the region-localized $C^{\alpha}-H$ bending (II) mode is shifted to lower wavenumbers by approximately 5 cm^{-1} in the 3_{10}-helix. This change in the wavenumber of the localized $C^{\alpha}-H$ bending (II) mode, together with the changes in the coupling constants discussed above, leads to the observed shift of the $C^{\alpha}-H$ bending (II) to lower wavenumbers in the calculated spectra.

This analysis shows that changes in the structure affect the positions of the bands in the extended amide III region in different way. First, structural changes influence the local electronic structure and bond strengths, which will affect the frequencies of the localized $C^{\alpha}-H$ bending and amide III modes. In particular the amide III modes can be expected to be very sensitive to changes in the strengths of the internal hydrogen bonds.[74] Second, structural changes influence the coupling between the localized $C^{\alpha}-H$ bending and amide III modes. While the coupling constant between the amide III and the $C^{\alpha}-H$ bending modes on the same residue can be expected to be sensitive to changes in the torsional angle φ, the coupling constant between the $C^{\alpha}-H$ bending modes and the amide III mode on the following residue can be expected to be sensitive to ψ. Third, also the coupling between the amide III modes on adjacent residues as well as the coupling between the $C^{\alpha}-H$ bending modes on such residues might be sensitive to structural changes. The analysis in terms of region-localized modes allows us to separate these different effects. However, in order to fully understand the different structural influences on the peaks in the extended amide III region, a more detailed analysis for a larger number of different structures will be necessary.

5. Conclusions

In this paper, we have applied our recently developed methodology for the analysis of calculated vibrational spectra in terms of localized modes[18] to study the IR and Raman spectra of the polypeptide $(Ala)_{20}$. In particular, we have analyzed the differences between the vibrational spectra of an α-helical and a 3_{10}-helical conformation. The localized modes, which are obtained from a unitary transformation of the normal modes belonging to one band or a specific region in the spectrum, are much simpler and therefore better suited for such an analysis than the normal modes. For the $(Ala)_{20}$ polypeptide considered here, the localized modes for one band in the vibrational spectrum form a set of modes that involve similar vibrations, each of them on a different amino acid residue, while the original normal modes are delocalized combinations of these localized modes.

Since the total IR and Raman intensities of a vibrational band are invariant under unitary transformations of the normal modes contributing to this band, the localized modes can be used to analyze these total intensities instead of the normal modes. Furthermore, since the localized modes each involve very similar atomic displacements on the different residues, they will in general each give a very similar contribution to the total intensity. Therefore, it is sufficient to consider one representative localized mode in order to analyze the total IR or Raman intensity of a certain vibrational band. This has been demonstrated for the Raman intensity of the amide II band, which shows a significantly larger intensity for the 3_{10}-helix than for the α-helix. By considering only the amide II localized mode on residue 12, which reflects the change in the total Raman intensity, the origin of this difference can be traced back to contributions of certain groups of atoms. We showed that the anisotropic Raman invariant γ, and particularly the contribution of the C−N vibration, are responsible for the increased amide II Raman intensity.

Furthermore, also the positions of the bands in the IR and Raman spectra can be analyzed in terms of localized modes. This feature has been employed to analyze the position of the amide I band, which in the 3_{10}-helix is shifted to lower wavenumbers by approximately 20 cm^{-1} compared to the α-helix. Two different contributions have to be considered in order to explain this shift. A part of this shift is accounted for by the shift of the vibrational frequencies of the localized amide I modes. The remaining part of the shift can be attributed to changes in the coupling constants. For the α-helix, the nearest-neighbor coupling constant is the largest, which leads to a shift of the highest-intensity modes to higher wavenumbers with respect to the vibrational frequencies of the localized modes. In the 3_{10}-helix, the second nearest-neighbor coupling constant is larger than the nearest-neighbor coupling constant, which leads to a different coupling pattern and results in a shift toward lower wavenumbers for the highest-intensity modes. More generally speaking, we show how the intensity distribution within one vibrational band can be explained in terms of the vibrational coupling matrix $\tilde{\mathbf{\Omega}}$, which determines how the localized modes couple to other localized modes, on the one hand and the intensity coupling matrix, which determines how the intensity is distributed among these coupled modes, on the other hand.

Finally, for the peaks found in the extended amide III region of the IR and Raman spectra of the two conformers of $(Ala)_{20}$ considered, we have demonstrated how the positions of these peaks can be analyzed. Two of the peaks in this region are mainly due to $C^{\alpha}-H$ bending vibrations, while the third one is mainly due to the classical amide III vibration (i.e., an in-phase combination of the N−H bending and the C−N stretching mode). However, the localized modes obtained for each of these bands show that there is a significant coupling between these modes. By performing the localization not for each band separately, but by localizing all normal modes in the extended amide III region at once, one obtains what we call region-localized modes, which are almost pure $C^{\alpha}-H$ bending and classical amide III vibrations, respectively. Using the region-localized modes, it is possible to extract vibrational frequencies of the pure $C^{\alpha}-H$ bending and classical amide III vibrations as well as coupling constants for the interaction between them. The positions in the extended amide III region can then be understood by both the differences in frequencies of the region-localized modes and by the differences in the coupling constants between them. It appears that the coupling constants describing couplings between different local vibrations are sensitive to different structural changes. While the coupling between the $C^{\alpha}-H$ bending modes and the classical amide III mode can be expected to depend on the backbone dihedral angle φ, the coupling between the $C^{\alpha}-H$ bending modes and the classical amide III mode on the following residue appears to be sensitive to changes in the backbone dihedral angle ψ. A detailed analysis of these couplings might lead to a better understanding of the dependence of vibrational frequencies observed in the extended amide III region on changes in the secondary structure.

However, it is not straightforward to extract general rules for relations between secondary structure and vibrational spectra from the results presented here. First, only two structural models

have been considered so far and the effects of different amino acid side chains were not investigated. Second, solvent or bulk effects have not been considered adequately. These will influence both the molecular structures and the vibrational frequencies. In particular, solvent effects will affect the various bands to a different extent and, for instance, in the extended amide III region solvent effects will change the separation between the $C^{\alpha}-H$ bending modes and the classical amide III mode, which might significantly change the resulting coupled normal modes. Such effects may be conveniently modeled in a microsolvation approach.

To conclude, the methodology studied in this work opens up the way to computational investigations studying the relation between secondary structure and vibrational spectra for large biomolecules. Such studies can be expected to yield a more detailed understanding of the complicated vibrational spectra of polypeptides and proteins than current studies using simplified model systems such as di- or tripeptides can provide. Furthermore, the analytic tools developed here will enable us to investigate how secondary structure determines the ROA spectra of polypeptides and proteins in detail. Work along these lines is currently in progress in our laboratory.

Acknowledgment. C.R.J. acknowledges funding by a Rubicon scholarship of The Netherlands Organization for Scientific Research (NWO). This work has been supported by the Swiss National Science Foundation SNF (Project 200020-121870).

Supporting Information Available: Cartesian coordinates of α-helical and 3_{10}-helical structures of $(Ala)_{20}$, details on the assignment of normal modes to vibrational bands, description and discussion of calculations including continuum solvation effects. This material is available free of charge via the Internet at http://pubs.acs.org.

References and Notes

(1) Carey, P. R. *J. Biol. Chem.* **1999**, *274*, 26625–26628.
(2) Thomas Jr, G. J. *Biopolymers* **2002**, *67*, 214–225.
(3) Vass, E.; Hollosi, M.; Besson, F.; Buchet, R. *Chem. Rev.* **2003**, *103*, 1917–1954.
(4) Barth, A. *Biochim. Biophys. Acta, Bioenerg.* **2007**, *1767*, 1073–1101.
(5) Keiderling, T. A. Peptide and Protein Conformational Studies with Vibrational Circular Dichroism and Related Spectroscopies. In *Circular Dichroism: Principles and Applications*, 2nd ed.; Berova, N., Nakanishi, K., Woody, R. W. Eds.; Wiley-VCH: New York, 2000.
(6) Zhu, F.; Isaacs, N. W.; Hecht, L.; Barron, L. D. *Structure* **2005**, *13*, 1409–1419.
(7) Herrmann, C.; Reiher, M. *Top. Curr. Chem.* **2007**, *268*, 85–132.
(8) Kubelka, J.; Silva, R. A. G. D.; Keiderling, T. A. *J. Am. Chem. Soc.* **2002**, *124*, 5325–5332.
(9) Blanch, E. W.; Hecht, L.; Day, L. A.; Pederson, D. M.; Barron, L. D. *J. Am. Chem. Soc.* **2001**, *123*, 4863–4864.
(10) Jacob, Ch. R.; Luber, S.; Reiher, M. *ChemPhysChem* **2008**, *9*, 2177–2180.
(11) Neugebauer, J.; Reiher, M.; Kind, C.; Hess, B. A. *J. Comput. Chem.* **2002**, *23*, 895–910.
(12) Herrmann, C.; Neugebauer, J.; Presselt, M.; Uhlemann, U.; Schmitt, M.; Rau, S.; Popp, J.; Reiher, M. *J. Phys. Chem. B* **2007**, *111*, 6078–6087.
(13) Herrmann, C.; Ruud, K.; Reiher, M. *ChemPhysChem* **2006**, *7*, 2189–2196.
(14) Reiher, M.; Neugebauer, J. *J. Chem. Phys.* **2003**, *118*, 1634–1641.
(15) Herrmann, C.; Neugebauer, J.; Reiher, M. *New J. Chem.* **2007**, *31*, 818–831.
(16) Kiewisch, K.; Neugebauer, J.; Reiher, M. *J. Chem. Phys.* **2008**, *129*, 204103.
(17) Luber, S.; Neugebauer, J.; Reiher, M. *J. Chem. Phys.* **2009**, *130*, 064105.
(18) Jacob, Ch. R.; Reiher, M. *J. Chem. Phys.* **2009**, *130*, 084106.
(19) Wilson, E. B.; Decius, J. C.; Cross, P. C. *Molecular Vibrations: The Theory of Infrared and Raman Vibrational Spectra*; Dover Publications: New York, 1980.
(20) Hug, W. *Chem. Phys.* **2001**, *264*, 53–69.
(21) Hug, W.; Haesler, J. *Int. J. Quantum Chem.* **2005**, *104*, 695–715.
(22) Long, D. A. *The Raman Effect: A Unified Treatment of the Theory of Raman Scattering by Molecules*; John Wiley & Sons: Chichester, 2001.
(23) Reiher, M.; Neugebauer, J.; Hess, B. A. *Z. Phys. Chem.* **2003**, *217*, 91–103.
(24) Ahlrichs, R. *Turbomole*. http://www.turbomole.com. Accessed January 12, 2009.
(25) Ahlrichs, R.; Bär, M.; Häser, M.; Horn, H.; Kölmel, Ch. *Chem. Phys. Lett.* **1989**, *162*, 165–169.
(26) Becke, A. D. *Phys. Rev. A* **1988**, *38*, 3098–3100.
(27) Perdew, J. P. *Phys. Rev. B* **1986**, *33*, 8822–8824.
(28) Schäfer, A.; Huber, C.; Ahlrichs, R. *J. Chem. Phys.* **1994**, *100*, 5829–5835.
(29) Turbomole basis set library. ftp://ftp.chemie.uni-karlsruhe.de/pub/basen. Accessed January 12, 2009.
(30) Eichkorn, K.; Treutler, O.; Öhm, H.; Häser, M.; Ahlrichs, R. *Chem. Phys. Lett.* **1995**, *240*, 283–289.
(31) Turbomole auxiliary basis sets. ftp://ftp.chemie.uni-karlsruhe.de/pub/jbasen. Accessed January 12, 2009.
(32) Neugebauer, J.; Herrmann, C.; Luber, S.; Reiher, M. SNF 4.0−A program for the quantum chemical calculation of vibrational spectra. http://www.theochem.ethz.ch/software/snf. Accessed January 12, 2009.
(33) Neugebauer, J.; Reiher, M.; Hess, B. A. *J. Chem. Phys.* **2002**, *117*, 8623–8633.
(34) Oliphant, T. Numpy−A python library for numerical computations. http://www.scipy.org/NumPy. Accessed January 12, 2009.
(35) The Open Babel package. http://openbabel.sourceforge.net/. Accessed January 12, 2009.
(36) Guha, R.; Howard, M. T.; Hutchison, G. R.; Murray-Rust, P.; Rzepa, H.; Steinbeck, Ch.; Wegner, J.; Willighagen, E. L. *J. Chem. Inf. Model* **2006**, *46*, 991–998.
(37) Jmol−An open-source molecule viewer. http://jmol.sourceforge.net. Accessed January 12, 2009.
(38) Mathplotlib−A Python 2D plotting library. http://matplotlib-.sourceforge.net/. Accessed January 12, 2009.
(39) Diem, M. *Introduction to Modern Vibrational Spectroscopy*; Wiley-Interscience: New York, 1993.
(40) Silva, R. A. G. D.; Kubelka, J.; Bour, P.; Decatur, S. M.; Keiderling, T. A. *Proc. Natl. Acad. Sci. U.S.A.* **2000**, *97*, 8318–8323.
(41) Krimm, S.; Bandekar, J. *Adv. Protein Chem.* **1986**, *38*, 181–364.
(42) Lee, S.-H.; Krimm, S. *Biopolymers* **1998**, *46*, 283–317.
(43) Toniolo, C.; Benedetti, E. *Macromolecules* **1991**, *24*, 4004–4009.
(44) Brehm, G.; Reiher, M.; Schneider, S. *J. Phys. Chem. A* **2002**, *106*, 12024–12034.
(45) Reiher, M.; Brehm, G.; Schneider, S. *J. Phys. Chem. A* **2004**, *108*, 734–742.
(46) Brehm, G.; Reiher, M.; Le Guennic, B.; Leibold, M.; Schindler, S.; Heinemann, F. W.; Schneider, S. *J. Raman Spectrosc.* **2006**, *37*, 108–122.
(47) Neugebauer, J.; Hess, B. A. *J. Chem. Phys.* **2003**, *118*, 7215–7225.
(48) Kubelka, J.; Huang, R.; Keiderling, T. A. *J. Phys. Chem. B* **2005**, *109*, 8231–8243.
(49) Bouř, P.; Sopková, J.; Bednárová, L.; Maloň, P.; Keiderling, T. A. *J. Comput. Chem.* **1997**, *18*, 646–659.
(50) Cramer, Ch. J.; Truhlar, D. G. *Chem. Rev.* **1999**, *99*, 2161–2200.
(51) Tomasi, J.; Mennucci, B.; Cammi, R. *Chem. Rev.* **2005**, *105*, 2999–3094.
(52) Klamt, A.; Schüürmann, G. *J. Chem. Soc., Perkin Trans.* **1993**, *2*, 799–805.
(53) Neugebauer, J.; Louwerse, M. J.; Baerends, E. J.; Wesolowski, T. A. *J. Chem. Phys.* **2005**, *122*, 094115.
(54) Neugebauer, J.; Jacob, Ch. R.; Wesolowski, T. A.; Baerends, E. J. *J. Phys. Chem. A* **2005**, *109*, 7805–7814.
(55) Jacob, Ch. R.; Neugebauer, J.; Jensen, L.; Visscher, L. *Phys. Chem. Chem. Phys.* **2006**, *8*, 2349–2359.
(56) Silva, R. A. G. D.; Yasui, S. C.; Kubelka, J.; Formaggio, F.; Crisma, M.; Toniolo, C.; Keiderling, T. A. *Biopolymers* **2002**, *65*, 229–243.
(57) Chi, Z.; Chen, X. G.; Holtz, J. S. W.; Asher, S. A. *Biochemistry* **1998**, *37*, 2854–2864.
(58) McColl, I. H.; Blanch, E. W.; Gill, A. C.; Rhie, A. G. O.; Ritchie, M. A.; Hecht, L.; Nielsen, K.; Barron, L. D. *J. Am. Chem. Soc.* **2003**, *125*, 10019–10026.
(59) Krimm, S.; Abe, Y. *Proc. Natl. Acad. Sci. U.S.A.* **1972**, *69*, 2788–2792.
(60) Moore, W. H.; Krimm, S. *Proc. Natl. Acad. Sci. U.S.A.* **1975**, *72*, 4933–4935.
(61) Torii, H.; Tasumi, M. *J. Chem. Phys.* **1992**, *96*, 3379–3387.
(62) Hamm, P.; Lim, M.; Hochstrasser, R. M. *J. Phys. Chem. B* **1998**, *102*, 6123–6138.
(63) Cha, S.; Ham, S.; Cho, M. *J. Chem. Phys.* **2002**, *117*, 740–750.
(64) Kubelka, J.; Kim, J.; Bour, P.; Keiderling, T. A. *Vib. Spectrosc.* **2006**, *42*, 63–73.

(65) Lord, R. C. *Appl. Spectrosc.* **1977**, *31*, 187–194.
(66) Overman, S. A.; Thomas, G. J., Jr. *Biochemistry* **1998**, *37*, 5654–5665.
(67) Asher, S. A.; Ianoul, A.; Mix, G.; Boyden, M. N.; Karnoup, A.; Diem, M.; Schweitzer-Stenner, R. *J. Am. Chem. Soc.* **2001**, *123*, 11775–11781.
(68) Mikhonin, A. V.; Ahmed, Z.; Ianoul, A.; Asher, S. A. *J. Phys. Chem. B* **2004**, *108*, 19020–19028.
(69) Mikhonin, A. V.; Bykov, S. V.; Myshakina, N. S.; Asher, S. A. *J. Phys. Chem. B* **2006**, *110*, 1928–1943.
(70) Oboodi, M. R.; Alva, C.; Diem, M. *J. Phys. Chem.* **1984**, *88*, 501–505.
(71) Diem, M.; Lee, O.; Roberts, G. M. *J. Phys. Chem.* **1992**, *96*, 548–554.
(72) Mirkin, N. G.; Krimm, S. *J. Phys. Chem. A* **2002**, *106*, 3391–3394.
(73) Schweitzer-Stenner, R.; Eker, F.; Huang, Q.; Griebenow, K.; Mroz, P. A.; Kozlowski, P. M. *J. Phys. Chem. B* **2002**, *106*, 4294–4304.
(74) Myshakina, N. S.; Ahmed, Z.; Asher, S. A. *J. Phys. Chem. B* **2008**, *112*, 11873–11877.

JP900354G